

# Monte-Carlo Simulations of Globular Cluster Evolution - II. Mass Spectra, Stellar Evolution and Lifetimes in the Galaxy.

Kriten J. Joshi<sup>1</sup>, Cody Nave<sup>2</sup>, and Frederic A. Rasio<sup>3,4</sup>

*Department of Physics, Massachusetts Institute of Technology*

## ABSTRACT

We study the dynamical evolution of globular clusters using our new 2-D Monte-Carlo code, and we calculate the lifetimes of clusters in the Galactic environment. We include the effects of a mass spectrum, mass loss in the Galactic tidal field, and stellar evolution. We consider initial King models containing  $N = 10^5 - 3 \times 10^5$  stars, with the dimensionless central potential  $W_0 = 1, 3$ , and  $7$ , and with power-law mass functions  $m^{-\alpha}$ , with  $\alpha = 1.5, 2.5$ , and  $3.5$ . The evolution is followed up to core collapse, or disruption, whichever occurs first.

We compare our results with those from similar calculations using 1-D Fokker-Planck methods. The disruption and core-collapse times of our models are significantly longer than those of the 1-D Fokker-Planck models. This is consistent with recent comparisons with direct  $N$ -body simulations, which have also shown that the 1-D Fokker-Planck models can significantly overestimate the escape rate from tidally truncated clusters. We find that our results are in very good agreement with recent 2-D Fokker-Planck calculations, for a wide range of initial conditions, although our Monte-Carlo models have a slightly lower mass loss rate. We find even closer agreement of our results with modified Fokker-Planck calculations that take into account the finite nature of the system.

In agreement with previous studies, our results show that the direct mass loss due to stellar evolution can significantly accelerate the mass loss rate through the tidal boundary, by reducing the binding energy of the cluster and making it expand. This effect causes most clusters with a low initial central concentration ( $W_0 \lesssim 3$ ) to disrupt quickly in the Galactic tidal field. The disruption is particularly rapid in clusters with a relatively flat mass spectrum. Only clusters born with high central concentrations ( $W_0 \gtrsim 7$ ), or with very steep initial mass functions ( $\alpha \gtrsim 3.5$ ) are likely to survive to the present and undergo core collapse. We identify the mechanism by which clusters disrupt

---

<sup>1</sup>6-218M MIT, 77 Massachusetts Ave, Cambridge, MA 02139; email: kjoshi@mit.edu.

<sup>2</sup>6-201 MIT, 77 Massachusetts Ave, Cambridge, MA 02139; email: cpnave@mit.edu.

<sup>3</sup>6-201 MIT, 77 Massachusetts Ave, Cambridge, MA 02139; email: rasio@mit.edu.

<sup>4</sup>Alfred P. Sloan Research Fellow.

as a dynamical instability in which the rate of mass loss increases catastrophically as the tidal boundary moves inward on the crossing timescale.

To understand the various processes that lead to the escape of stars, we study the velocity distribution and orbital characteristics of escaping stars. We find that the velocity distribution of escaping stars in collapsing clusters is significantly different from the distribution in disrupting clusters. We also compute the lifetime of a cluster on an eccentric orbit in the Galaxy, such that it fills its Roche lobe only at perigalacticon. We find that such an orbit can extend the disruption time by at most a factor of a few compared to a circular orbit in which the cluster fills its Roche lobe at all times.

*Subject headings:* cluster: globular — celestial mechanics, stellar dynamics — Monte-Carlo

## 1. Introduction

The development of numerical methods for simulating the dynamical evolution of dense star clusters started in the 1970's with Monte-Carlo techniques (Henon 1971a,b; Spitzer 1987, and references therein), and several groups applied these techniques to address problems related to the evolution of globular clusters. A method based on the direct numerical integration of the Fokker-Planck equation in phase space was later developed by Cohn (1979, 1980). The Fokker-Planck (hereafter F-P) methods have since been greatly improved, and they have been extended to more realistic simulations that take into account (approximately) the presence of a mass spectrum, primordial binaries, tidal boundaries, gravitational shock heating by the galactic disk and bulge, and mass loss due to stellar evolution (see Meylan & Heggie 1997 for a recent review). Direct  $N$ -body simulations can also be used to study globular cluster dynamics, but, until recently, they have been limited to rather unrealistic systems containing very low numbers of stars. The GRAPE family of special-purpose computers now make it possible to perform direct  $N$ -body integrations for clusters containing up to  $N \sim 32,000$  single stars, although the computing time for such large simulations remains considerable (see Makino et al. 1997, and references therein). This is the second of a series of papers in which we study globular cluster dynamics using a Monte-Carlo technique similar to the original Henon (1971b) method. Parallel supercomputers now make it possible to perform Monte-Carlo simulations for the dynamical evolution of dense stellar systems containing up to  $N \sim 10^5 - 10^6$  stars in less than  $\sim 1$  day of computing time.

The evolution of globular clusters in the Galactic environment has been studied using a variety of theoretical and numerical techniques over. The first comprehensive study of cluster lifetimes was conducted by Chernoff & Weinberg (1990, hereafter CW) using F-P simulations. They included the effects of a power-law mass spectrum, a tidal cut-off radius imposed by the tidal field of the Galaxy, and mass loss due to stellar evolution. Their results were surprising, and far reaching, since they showed for the first time that the majority of clusters with a wide range of initial conditions would be

disrupted in  $\lesssim 10^{10}$  yr, and would not survive until core collapse. CW carried out their calculations using a 1-D F-P method, in which the stellar distribution function in phase space is assumed to depend on the orbital energy only. However, more recently, similar calculations undertaken using direct  $N$ -body simulations gave cluster lifetimes up to an order of magnitude longer compared to those computed by CW (Fukushige & Heggie 1995; Portegies Zwart et al. 1998). The discrepancy appears to be caused by an overestimated mass loss rate in the 1-D F-P formulation (Takahashi & Portegies Zwart 1998), which does not properly account for the velocity anisotropy in the cluster. To overcome this problem, new 2-D versions of the F-P method (in which the distribution function depends on both energy and angular momentum) have been employed (Takahashi 1995, 1996, 1997; Drukier et al. 1999).

The 2-D F-P models provide cluster lifetimes in significantly better agreement with direct  $N$ -body integrations (Takahashi & Portegies Zwart 1998). However, the 2-D F-P models still exhibit a slightly higher mass loss rate compared to  $N$ -body simulations. This may result from the representation of the system in terms of a continuous distribution function in the F-P formulation, which effectively models the behavior of the cluster in the  $N \rightarrow \infty$  limit. To test this possibility, Takahashi & Portegies Zwart (1998) introduce an additional free parameter  $\nu_{\text{esc}}$  in their F-P models, attempting to take into account the finite ratio of the crossing time to the relaxation time (see also Lee & Ostriker 1987; Ross et al. 1997). They use this free parameter to lower the overall mass loss rate in their F-P models and obtain agreement with  $N$ -body simulations (performed with up to  $N = 32,768$ ). Takahashi & Portegies Zwart (1999, hereafter TPZ) show that, after calibration, a single value of  $\nu_{\text{esc}}$  gives consistent agreement with  $N$ -body simulations for a broad range of initial conditions .

The first paper in this series presented details about our new parallel Monte-Carlo code as well as the results of a series of initial test calculations (Joshi, Rasio & Portegies Zwart 1999, hereafter Paper I). We found excellent agreement between the results of our test calculations and those of direct  $N$ -body and 1-D Fokker-Planck simulations for a variety of single-component clusters (i.e., containing equal-mass stars). However, we found that, for tidally truncated clusters, the mass loss rate in our models was significantly lower, and the core-collapse times significantly longer, than in corresponding 1-D F-P calculations. We noted that, for a single case (a  $W_0 = 3$  King model), our results were in good agreement with those of 2-D F-P calculations by Takahashi (1999).

In this paper, we extend our Monte-Carlo calculations to multi-component clusters (described by a continuous, power-law stellar mass function), and we study the evolution of globular clusters with a broad range of initial conditions. Our calculations include an improved treatment of mass loss through the tidal boundary, as well as mass loss due to stellar evolution. Our new method treats the mass loss through the tidal boundary more carefully in part by making the timestep smaller, especially in situations where the tidal mass loss can lead to an instability resulting in rapid disruption of the cluster. We also account for the shrinking of the tidal boundary in each timestep by iteratively removing stars with apocenter distances greater than the tidal boundary, and recomputing the tidal radius using the new (lower) mass of the cluster. We compare our

new results with those of CW and TPZ. We also go beyond these previous studies and explore several other issues relating to the pre-collapse evolution of globular clusters. We study in detail the importance of the velocity anisotropy in determining the stellar escape rate. We also compare the orbital properties of escaping stars in disrupting and collapsing clusters. Finally, we consider the effects of an eccentric orbit in the Galaxy, allowing for the possibility that a cluster may not fill its Roche lobe at all points in its orbit.

The calculations presented in this paper are for clusters containing single stars only. The dynamical effects of hard primordial binaries for the overall cluster evolution are not significant during most of the the *pre-collapse* phase. Energy generation through binary – single star and binary – binary interactions becomes significant only when the cluster approaches core collapse and interaction rates in the core increase substantially (Hut, McMillan & Romani 1992; Gao et al. 1991; McMillan & Hut 1994). Formation of hard “three-body” binaries can also be neglected until the cluster reaches a deep core-collapse phase. During the pre-collapse evolution, hard binaries behave approximately like single more massive stars, while soft binaries (which have a larger interaction cross section) may be disrupted. Since we do not include the effects of energy generation by primordial binaries in our calculations, the (well-defined) core-collapse times presented here may be re-interpreted as corresponding approximately to the onset of the “binary-burning” phase, during which a similar cluster containing binaries would be supported in quasi-equilibrium by energy-generating interactions with hard binaries in its core (Spitzer & Mathieu 1980; Goodman & Hut 1989; McMillan, Hut & Makino 1990). Our calculations of disruption times (for clusters that disrupt in the tidal field of the Galaxy before reaching core collapse) are largely independent of the cluster binary content, since the central densities and core interaction rates in these clusters always remain very low.

Our paper is organized as follows. In §2, we describe the treatment of tidal stripping and mass loss due to stellar evolution in our Monte-Carlo models, along with a discussion of the initial conditions for our simulations. In §3, we present the results of our simulations and comparisons with F-P calculations. In §4, we summarize our results.

## 2. Monte-Carlo Method

Our code, described in detail in Paper I, is based on the orbit-averaged Monte-Carlo method first developed by Hénon (1971a,b). Although in Paper I we only presented results of test calculations performed for single-component clusters, the method is completely general, and the implementation of an arbitrary mass spectrum is straightforward. This section describes additional features of our code that were not included in Paper I: an improved treatment of mass loss through the tidal boundary (§2.1), and a simple implementation of stellar evolution (§2.2). The construction of initial multi-component King models for our study of cluster lifetimes is described in §3.3. The highly simplified treatments of tidal effects and stellar evolution adopted here are for consistency with previous studies, since our intent in this paper is still mainly to establish the accuracy of

our code by presenting detailed comparisons with the results of other methods. In future work, however, we intend to implement more sophisticated and up-to-date treatments of these effects.

### 2.1. Tidal Stripping of Stars

In an isolated cluster, the mass loss rate (up to core collapse) is relatively small, since escaping stars must acquire positive energies mostly through rare, strong interactions in the dense cluster core (see the discussion in Paper I, §3.1). In contrast, for a tidally truncated cluster, the mass loss is dominated by diffusion across the tidal boundary (also referred to as “tidal stripping”). In our Monte-Carlo simulations, a star is assumed to be tidally stripped from the cluster (and lost instantaneously) if the *apocenter* of its orbit in the cluster is outside the tidal radius. This is in contrast to the *energy-based* escape criterion that is used in 1-D F-P models, where a star is considered lost if its energy is greater than the energy at the tidal radius, regardless of its angular momentum. As noted in Paper I, the 2-D treatment is crucial in order to avoid overestimating the escape rate, since stars with high angular momentum, i.e., on more circular orbits, are less likely to be tidally stripped from the cluster than those (with the same energy) on more radial orbits.

A subtle, yet important aspect of the mass loss across the tidal boundary, is the possibility of the tidal stripping process becoming *unstable* if the tidal boundary moves inward too quickly. As the total mass of the cluster decreases through the escape of stars, the tidal radius of the cluster shrinks. This causes even more stars to escape, causing the tidal boundary to shrink further. If at any time during the evolution of the cluster the density gradient at the tidal radius is too large, this can lead to an unstable situation, in which the tidal radius continues to shrink on the dynamical timescale, causing the cluster to disrupt. The development of this instability characterizes the final evolution of all clusters with a low initial central concentration that disrupt in the Galactic tidal field before reaching core collapse.

We test for this instability at each timestep in our simulations, by iteratively removing escaping stars and recomputing the tidal radius with the appropriately lowered cluster mass. For stable models, this iteration converges quickly, giving a finite escape rate. Even before the development of the instability, this iterative procedure must be used for an accurate determination of the mass loss rate. When the mass loss rate due to tidal stripping is high, we also impose a timestep small enough that no more than 1% of the total mass is lost in a single timestep. This is to ensure that the potential is updated frequently enough to take the mass loss into account. This improved treatment of tidal stripping was not used in our calculations for Paper I. However, all the results presented in Paper I were for clusters with equal-mass stars, with no stellar evolution. Under those conditions, all models reach core collapse, with no disruptions. The issue of unstable mass loss is not significant in those cases, and hence the results of Paper I are unaffected.

## 2.2. Stellar Evolution

Our simplified treatment follows those adopted by CW and TPZ. We assume that a star evolves instantaneously to become a compact remnant at the end of its main-sequence lifetime. Indeed, since the evolution of our cluster models takes place on the relaxation timescale (i.e., the timestep is a fraction of the relaxation time  $t_r \gtrsim 10^9$  yr), while the dominant mass loss phase during late stages of stellar evolution takes place on a much shorter timescale ( $\sim 10^6$  yr), the mass loss can be considered instantaneous. We neglect mass losses in stellar winds for main-sequence stars. We assume that the main-sequence lifetime and remnant mass is a function of the initial stellar mass only. Table 1 shows the main-sequence lifetimes of stars with initial masses up to  $15 M_\odot$ , and the corresponding remnant masses. In order to facilitate comparison with F-P calculations (CW, and TPZ), we use the same lifetimes and remnant masses as CW. For stars of mass  $m < 4 M_\odot$ , the remnants are white dwarfs of mass  $0.58 + 0.22(m - 1)$ , while for  $m > 8 M_\odot$ , the remnants are neutron stars. Stars with intermediate masses are completely destroyed (Iben & Renzini 1983). The lowest initial mass considered by CW was  $\simeq 0.83 M_\odot$ . For lower mass stars, in order to maintain consistency with TPZ, we extrapolate the lifetimes assuming a simple  $m^{-3.5}$  scaling (Drukier 1995). We interpolate the values given in Table 1 using a cubic spline to obtain lifetimes for stars with intermediate masses, up to  $15 M_\odot$ . In our initial models (see §2.3), we assign masses to stars according to a continuous power-law distribution. This provides a natural spread in their lifetimes, and avoids having large numbers of stars undergoing identical stellar evolution. In contrast, in F-P calculations, the mass function is approximated by 20 discrete logarithmically spaced mass bins over the entire range of masses. The mass in each bin is then reduced linearly in time from its initial mass to its final (remnant) mass, over a time interval equal to the maximum difference in main-sequence lifetimes spanned by the stars in that mass bin (see TPZ for further details). This has the effect of averaging the effective mass loss rate over the masses in each bin.

We assume that all stars in the cluster were formed in the same star formation epoch, and hence all stars have the same age throughout the simulation. During each timestep, all the stars that have evolved beyond their main-sequence lifetimes are labelled as remnants, and their masses are changed accordingly. In the initial stages of evolution ( $t \lesssim 10^8$  yr), when the mass loss rate due to stellar evolution is highest, care is taken to make the timestep small enough so that no more than 1% of the total mass is lost in a single timestep. This is to ensure that the system remains very close to virial equilibrium through this phase.

## 2.3. Initial Models

The initial condition for each simulation is a King model with a power-law mass spectrum. In order to facilitate comparison with the F-P calculations of CW and TPZ, we select the same set of initial King models for our simulations, with  $W_0 = 1, 3$ , and  $7$ . Most of our calculations were performed with  $N = 10^5$  stars, with a few calculations repeated with  $N = 3 \times 10^5$  stars

and showing no significant differences in the evolution. We construct the initial model by first generating a single-component King model with the selected  $W_0$ . We then assign masses to the stars according to a power-law mass function

$$f(m) \propto m^{-\alpha}, \quad (1)$$

with  $m$  between  $0.4 M_\odot$  and  $15 M_\odot$ . We consider three different values for the power-law index  $\alpha = 1.5, 2.5$ , and  $3.5$ , assuming no initial mass segregation. Although this method of generating a multi-component initial King model is convenient and widely used to create initial conditions for numerical work (including  $N$ -body, F-P, and Monte-Carlo simulations), the resulting initial model is not in strict virial equilibrium since the masses are assigned independently of the positions and velocities of stars. However, we find that the initial clusters relax to virial equilibrium within just a few timesteps in our simulations. Virial equilibrium is then maintained to high accuracy during the entire calculation, with the virial ratio  $2T/|W| = 1$  to within  $< 1\%$ .

In addition to selecting the dimensionless model parameters  $W_0$ ,  $N$ , and  $\alpha$  (which specify the initial dynamical state of the system), we must also relate the dynamical timescale with the stellar evolution timescale for the system. The basic unit of time in our models is scaled to the relaxation time. Since the stellar evolution timescale is not directly related to the dynamical timescale, the lifetimes of stars (in years) cannot be computed directly from our code units. Hence, in order to compute the mass loss due to stellar evolution, we must additionally relate the two timescales by converting the evolution time to physical units. To maintain consistency with F-P calculations, we use the same prescription as CW. We assume a value for the initial relaxation time of the system, which is defined as follows:

$$t_r = 2.57 F \text{ [Myr]}, \quad (2)$$

where

$$F \equiv \frac{M}{M_\odot \text{ kpc}} \frac{220 \text{ km s}^{-1}}{v_g} \frac{1}{\ln N}. \quad (3)$$

Here  $M$  is the total mass of the cluster,  $R_g$  is its distance to the Galactic center (assuming a circular orbit),  $v_g$  is the circular speed of the cluster, and  $N$  is the total number of stars. (This expression for the relaxation time is derived from CW’s eqs. [1], [2], and [6] with  $m = M_\odot$ ,  $r = r_t$ , and  $c_1 = 1$ .) Following CW, a group of models with the same value of  $F$  (constant relaxation time) at the beginning of the simulation is referred to as a “Family.” Our survey covers CW’s Families 1, 2, 3 and 4. For each value of  $W_0$  and  $\alpha$ , we consider four different models, one from each Family.

To convert from our code units, or “virial units” (see Paper I, §2.8 for details) to physical units, we proceed as follows. For a given Family (i.e., a specified value of  $F$ ), cluster mass  $M$ , and  $N$ , we compute the distance to the Galactic center  $R_g$  using equation (3). The circular velocity of  $220 \text{ km s}^{-1}$  for the cluster (combined with  $R_g$ ) then provides an inferred value for the mass of the Galaxy  $M_g$  contained within the cluster orbit. Using  $M$ ,  $M_g$ , and  $R_g$ , we compute the tidal radius for the cluster, as  $r_t = R_g (M/3M_g)^{1/3}$ , in physical units (pc). The ratio of the tidal radius to the virial radius (i.e.,  $r_t$  in code units) for a King model depends only on  $W_0$ , and hence is known for

the initial model. This gives the virial radius in pc. The unit of mass is simply the total initial cluster mass  $M$ . Having expressed the units of distance and mass in physical units, the unit of evolution time (which is proportional to the relaxation time) can easily be converted to physical units (yr) using equation (31) from Paper I.

Table 2 shows the value of  $F$  for the four selected Families. For reference, we also give the relaxation time at the half-mass radius  $t_{\text{rh}}$  for the models with  $W_0 = 3$  and  $\alpha = 2.5$  (mean stellar mass  $\bar{m} \simeq 1 \text{ M}_\odot$ ), which we compute using the standard expression (see, e.g., Spitzer 1987),

$$t_{\text{rh}} = 0.138 \frac{N^{1/2} r_{\text{h}}^{3/2}}{\bar{m}^{1/2} G^{1/2} \ln N}, \quad (4)$$

where  $r_{\text{h}}$  is the half-mass radius of the cluster.

### 3. Results

In Paper I we presented our first results for the evolution of single-component clusters up to core collapse. We computed core-collapse times for the entire sequence of King models ( $W_0 = 1 - 12$ ), including the effects of a tidal boundary. Here we extend our study to clusters with a power-law mass spectrum, and mass loss due to stellar evolution.

#### 3.1. Qualitative Effects of Tidal Mass Loss and Stellar Evolution

We begin by briefly reviewing the evolution of single-component, tidally truncated systems. In Figure 1, we show the core-collapse times for King models with  $W_0 = 1 - 12$  (Paper I). The core-collapse times for tidally truncated models are compared with equivalent isolated models. Although the isolated models also begin as King models with a finite tidal radius, the tidal boundary is not enforced during their evolution, allowing the cluster to expand freely. The most notable result is that the maximum core-collapse time for the tidally truncated clusters occurs at  $W_0 \simeq 5$ , compared to  $W_0 = 1$  for isolated clusters. This is because the low  $W_0$  King models have a less centrally concentrated density profile, and hence a higher density at the tidal radius compared to the high  $W_0$  models. This leads to higher mass loss through the tidal boundary, which reduces the mass of the cluster and shortens the core-collapse time. This effect is further complicated by the introduction of a non-trivial mass spectrum, and mass loss due to stellar evolution in the cluster.

In Figure 2, we show a comparison of the mass loss rate due to the tidal boundary, a power-law mass spectrum, and stellar evolution. We consider the evolution of a  $W_0 = 3$  King model, in four different environments. All models considered in this comparison belong to Family 1 (cf. §2.2). We first compare an isolated, single component model (without an enforced tidal boundary), and a tidally truncated model (as in fig. [1]). Clearly, the presence of the tidal boundary is responsible for almost all the mass loss from the cluster, and greatly reduces the core-collapse time. Introducing a

power-law mass spectrum further reduces the core-collapse time, since mass segregation increases the core density, and accelerates the development of the gravothermal instability. The shorter core-collapse time reduces the total loss through the tidal boundary by leaving less time for relaxation in the outer regions, and also lowering the density in the outer regions through mass segregation. This results in a higher final mass compared to the single-component system. Finally, allowing mass loss through stellar evolution causes even faster overall mass loss, which eventually disrupts the system. The introduction of a Salpeter-like power-law initial mass function ( $\alpha = 2.5$ ) is sufficient to cause this cluster to disrupt before core collapse.

The presence of a tidal boundary causes stars on radial orbits in the outer regions of the cluster to be preferentially removed. This produces a significant anisotropy in the outer regions as the cluster evolves. As noted in Paper I, a proper treatment of this anisotropy is essential in computing the mass loss rate. A star in an orbit with low angular momentum has a larger apocenter distance compared to a star (with the same energy) in a high angular momentum orbit. Hence stars in low angular momentum (i.e., radial) orbits are preferentially lost through the tidal boundary, causing an anisotropy to develop in the cluster. In 1-D F-P models, this is not taken into account, and therefore 1-D F-P models predict a much larger mass loss compared to 2-D models. In Figure 3, we show the anisotropy parameter  $\beta = 1 - \sigma_t^2/\sigma_r^2$ , for a  $W_0 = 3$  King model ( $\alpha = 2.5$ , Family 1), at two different times during its evolution. Here,  $\sigma_t$  and  $\sigma_r$  are the 1-D tangential and radial velocity dispersions, respectively. The initial King model is isotropic. At later times, the anisotropy in the outer region grows steadily as the tidal radius moves inward.

Another consequence of mass loss and stellar evolution is the gradual flattening of the stellar mass function as the cluster evolves. In Figure 4, we show the mass spectrum in the core and at the half-mass radius of a  $W_0 = 3$  King model ( $\alpha = 2.5$ , Family 1), at two different times during its evolution. Since the heavier stars concentrate in the core, and have lower mean velocities, the mass loss across the tidal boundary occurs preferentially for the lighter stars. This leads to a gradual flattening of the overall mass function of the cluster. However, this picture is somewhat complicated by stellar evolution, which continuously depletes high mass stars from the cluster. The remaining heavier stars gradually accumulate in the inner regions as the cluster evolves. We see the expected flattening of the mass spectrum for  $m \lesssim 2M_\odot$ , and the rapid depletion of the high mass stars due to stellar evolution.

### 3.2. Cluster Lifetimes: Comparison with Fokker-Planck results

We now present our survey of cluster lifetimes, and we compare our results with equivalent 1-D and 2-D F-P results. For each combination of  $W_0$  and  $\alpha$ , we perform four different simulations (Families 1 – 4), corresponding to different initial relaxation times (cf. Table [2]). We follow the evolution until core collapse, or disruption, whichever occurs first. We also stop the computation if the total bound mass decreases below 2% of the initial mass, and consider the cluster to be disrupted in such cases. We compare our results with those of two different F-P studies: the 1-D

F-P calculations of Chernoff & Weinberg (1990, CW), and the more recent 2-D calculations of Takahashi & Portegies Zwart (1999, TPZ).

### 3.2.1. Comparison with 1-D Fokker-Planck models

Table 3 compares the our Monte-Carlo (MC) models with the 1-D F-P calculations conducted by CW. Following the same notation as CW, the final core collapse of a cluster is denoted by ‘C’, and disruption is denoted by ‘D’. The final mass of the cluster (in units of the initial mass) and the lifetime in units of  $10^9$  yr (time to disruption or core collapse) are also given. The evolution of clusters that reach core collapse is not followed beyond the core-collapse phase. For disrupting clusters, CW provide a value for the final mass, which corresponds to the point at which the tidal mass loss becomes unstable and the cluster disrupts on the dynamical timescale. However, we find that the point at which the instability develops depends sensitively on the method used for computing the tidal mass loss and requires the potential to be updated on a very short timescale. In this regime, since the system evolves (and disrupts) on the dynamical timescale, the orbit-averaged approximation used to solve the Fokker-Planck equation also breaks down. This is true for both Monte-Carlo and F-P simulations. The only way to determine the point of instability reliably is to follow the evolution on the dynamical timescale using direct  $N$ -body integrations. Hence, for disrupting models, we quote the final mass as zero, and only provide the disruption time (which can be determined very accurately).

We find that *all* our Monte-Carlo models disrupt later than those of CW. However, for models that undergo core collapse, the core-collapse times are earlier in some cases compared to CW. The discrepancy in the disruption times sometimes exceeds an order of magnitude (e.g.,  $W_0 = 1$ ,  $\alpha = 2.5$ ). On the other hand, the discrepancy in the lifetime of the clusters with  $\alpha = 1.5$  and  $W_0 = 1$  and those with  $W_0 = 3$  is only a factor of three. These models disrupt very quickly and the a proper treatment of anisotropy does not extend their lifetimes very much, since the combination of a flat initial mass function and a shallow initial potential leads to rapid disruption.

Out of 36 models, we find that half (18) of our Monte-Carlo models reach core collapse before disruption, compared to fewer than 30% (10) of models in the CW survey. The longer lifetimes of our models allow more of the clusters to reach core collapse in our simulations. All the clusters that experience core collapse according to CW also experience core collapse in our calculations. Since the main difference between our models and those of CW comes from the different mass loss rates, we predictably find that our results match more closely those of CW in all cases where the overall mass loss up to core collapse is relatively small. For example, the more concentrated clusters ( $W_0 = 7$ ) with steep mass functions ( $\alpha = 2.5$  and 3.5) show very similar behavior, with the discrepancy in final mass and core-collapse time being less than a factor of two. However, we cannot expect complete agreement even in these cases, since the effects of anisotropy cannot be completely ignored.

The overall disagreement between our Monte-Carlo models and 1-D F-P models is very significant. This was also evident in some of the results presented in Paper I, where we compared core-collapse times for tidally truncated single-component King models, with 1-D F-P calculations by Quinlan (1996). This discrepancy has also been noted by Takahashi & Portegies Zwart (1998), and Portegies Zwart et al. (1998). The improved 2-D F-P code developed by Takahashi (1995, 1996, 1997) is now able to properly account for the anisotropy, allowing a more meaningful comparison with other 2-D calculations, including our own.

### 3.2.2. Comparison with 2-D Fokker-Planck models

Comparisons of the mass loss evolution is shown in Figures 5, 6, and 7, where the solid lines show our Monte-Carlo models, and the dashed lines show the 2-D F-P models from TPZ.

In Figure 5, we show the evolution of  $W_0 = 1$  King models. The very low initial central density of these models makes them very sensitive to the tidal boundary, leading to very rapid mass loss. As a result, all the  $W_0 = 1$  models disrupt without ever reaching core collapse. In addition, these models demonstrate the largest variation in lifetimes depending on their initial mass spectrum. For a relatively flat mass function ( $\alpha = 1.5$ ), the disruption time is less than  $3 \times 10^7$  yr. The large fraction of massive stars in these models, combined with the shallow initial central potential, leads to very rapid mass loss and complete disruption. For a more realistic, Salpeter-like initial mass function ( $\alpha = 2.5$ ), the  $W_0 = 1$  models have a longer lifetime, but still disrupt in  $\lesssim 10^9$  yr. The  $\alpha = 3.5$  models have very few massive stars, and hence behave almost like models without stellar evolution. We see that it is only with such a steep mass function, that the  $W_0 = 1$  models can survive until the present epoch ( $\gtrsim 10^{10}$  yr). We also find that the Family 1 and 2 models can just barely reach core collapse, despite having lost most of their mass. The Family 3 and 4 models are disrupted, having slightly higher mass loss rates.

We see very good agreement throughout the evolution between our Monte-Carlo models and the 2-D F-P models. In all cases, the qualitative behaviors indicated by the two methods are identical, even though the Monte-Carlo models consistently have somewhat longer lifetimes than the F-P models. The average discrepancy in the disruption times for all models is approximately a factor of two. The discrepancy in disruption times is due to a slightly lower mass loss rate in our models, which allows the clusters to live longer. Since the F-P calculations correspond to the  $N \rightarrow \infty$  limit, they tend to overestimate the overall mass loss rate (we discuss this issue in more detail in the next section). This tendency has been pointed out by Takahashi & Portegies Zwart (1998), who compared the results of 2-D F-P simulations with those of direct  $N$ -body simulations with up to  $N = 32,768$ . They have attempted to account for the finiteness of the system in their F-P models by introducing an additional parameter in their calculations to modify the mass loss rate. The comparison shown in Figures 5, 6 and 7 is for the unmodified  $N \rightarrow \infty$  F-P models.

We find complete agreement with TPZ in distinguishing models that reach core collapse from

those that disrupt. The only case in which there is some ambiguity is the  $W_0 = 1, \alpha = 3.5$ , Family 2 model, which collapses in our calculations, while TPZ indicate disruption. This is clearly a borderline case, in which the cluster reaches core collapse just prior to disruption in our calculation. Since the cluster has lost almost all its mass at core collapse, the distinction between core collapse and disruption is largely irrelevant. It is important to note, however, that we find the boundary between collapsing and disrupting models at almost exactly the same location in parameter space ( $W_0$ ,  $\alpha$ , and relaxation time) as TPZ. This agreement is as significant, if not more, than the comparison of final masses and disruption times.

In Figure 6, we show the comparison of  $W_0 = 3$  King models. Again, the overall agreement is very good, except for the later disruption times for the Monte-Carlo models. The most notable difference from the  $W_0 = 1$  models, is that the  $W_0 = 3$  models clearly reach core collapse prior to disruption for  $\alpha = 3.5$ . The core collapse times for the  $\alpha = 3.5$  models are very long ( $\gtrsim 3 \times 10^{10}$  yr), with only a small fraction of the initial mass remaining bound at core collapse. Again, we find excellent agreement between the qualitative behaviors of the F-P and Monte-Carlo models.

In Figure 7, we show the evolution of the  $W_0 = 7$  King models. In the presence of a tidal boundary, the  $W_0 \simeq 5$  King models have the distinction of having the longest core-collapse times (see Fig. 1). This is because they begin with a sufficiently high initial core density, and do not expand very much before core collapse. Hence, the mass loss through the tidal boundary is minimal. King models with a lower  $W_0$  lose more mass through the tidal boundary, and evolve more quickly toward core collapse or disruption, while models with higher  $W_0$  have very high initial core densities, leading to short core-collapse times. All our  $W_0 = 7$  models reach core collapse. Even the models with a relatively flat mass function ( $\alpha = 1.5$ ) achieve core collapse, although the final bound mass in that case is very small. We again see good overall agreement between the Monte-Carlo and F-P models. In the next section, we discuss the possible reasons for the small discrepancy in the mass loss rate between the Monte-Carlo and F-P models.

### 3.2.3. Comparison with finite Fokker-Planck models

We first highlight some of the general issues relating to mass loss in the systems we have considered. In Figure 8, we show the relative rates of mass loss due to stellar evolution and tidal stripping, for  $W_0 = 1, 3$ , and  $7$  King models, with different mass spectra ( $\alpha = 1.5, 2.5$ , and  $3.5$ ). We see that stellar evolution is most significant in the early phases, while tidal mass loss dominates the evolution in the later phases. The relative importance of stellar evolution depends on the fraction of massive stars in the cluster, which dominate the mass loss early in the evolution. Hence, the  $\alpha = 1.5$  models suffer the greatest mass loss due to stellar evolution, accounting for up to 50% of the total mass loss in some cases (e.g.,  $W_0 = 7, \alpha = 1.5$ ). All models shown belong to Family 2. It is important to note the large variation in the timescales, and in the relative importance of stellar evolution versus tidal mass loss across all models.

Through comparisons with  $N$ -body simulations, Takahashi & Portegies Zwart (1998) have argued that assuming  $N \rightarrow \infty$  leads to an overestimate of the mass loss rate due to tidal stripping of stars. To compensate for this, they introduce a free parameter  $\nu_{\text{esc}}$  in their calculations, to account for the finite time (of the order of the crossing time) it takes for an escaping star to leave the cluster. They calibrate this parameter through comparisons with  $N$ -body simulations, for  $N = 1,024 - 32,768$ . Since for low  $N$ , the  $N$ -body models are too noisy, and the F-P models are insensitive to  $\nu_{\text{esc}}$  for large  $N$ , TPZ find that the calibration is most suitably done using  $N \sim 16,000$  (for further details, see the discussion by TPZ). They show that a single value of this parameter gives good agreement with  $N$ -body simulations for a wide range of initial conditions. Using this prescription, TPZ provide results of their calculations for finite clusters with  $N = 3 \times 10^5$  in addition to their  $N \rightarrow \infty$  results. They find that their finite models, as expected, have lower mass loss rates, and consequently longer lifetimes compared to their infinite models.

In Table 4, we compare the results of our Monte-Carlo calculations with  $N = 3 \times 10^5$  stars with the finite and infinite F-P models of TPZ. We consider four cases:  $W_0 = 1$  and  $3$ , Families 1 and 4,  $\alpha = 2.5$ . All finite TPZ models have longer lifetimes than their infinite models. However, there is practically no difference between their finite and infinite models for core-collapsing clusters. Hence we focus our attention only on the disrupting models. We see that in all four cases, the longer lifetimes of the finite models are in better agreement with our Monte-Carlo results, although the agreement is still not perfect. The largest difference between the finite and infinite F-P models is for  $W_0 = 1$ , Family 4, in which case the Monte-Carlo result lies in between the finite and infinite F-P results. In the remaining cases, the Monte-Carlo disruption times are longer than those of the finite F-P models.

Both Monte-Carlo and F-P methods are based on the orbit-averaged Fokker-Planck approximation, which treats all interactions in the weak scattering limit, i.e., it does not take into account the effect of strong encounters. Both methods compute the *cumulative* effect of distant encounters in one timestep (which is a fraction of the relaxation time). In this approximation, events on the crossing timescale (such as the escape of stars) are treated as being instantaneous. Since the relaxation time is proportional to  $N / \ln N$  times the crossing time, this is equivalent to assuming  $N \rightarrow \infty$  in the F-P models. However, in our Monte-Carlo models, there is *always* a finite  $N$ , since we maintain a discrete representation of the cluster at all times and follow the same phase space parameters as in an  $N$ -body simulation. Thus, although both methods make the same assumption about the relation between the crossing time and relaxation time, for all other aspects of the evolution, the Monte-Carlo models remain finite. This automatically allows most aspects of cluster evolution, including the escape of stars, stellar evolution, and computation of the potential, to be handled on a discrete, star-by-star basis. On the other hand, the F-P models use a few coarsely binned individual mass components represented by continuous distribution functions (consistent with  $N \rightarrow \infty$ ) to model all processes. In this sense, the Monte-Carlo models can be regarded as being intermediate between direct  $N$ -body simulations and F-P models.

The importance of using the correct value of  $N$  in dynamical calculations for realistic cluster

models has also been demonstrated through  $N$ -body simulations, which show that the evolution of finite clusters scales with  $N$  in a rather complex way (see Portegies Zwart et al. 1998 and the “Collaborative Experiment” by Heggie et al. 1999). Hence, despite correcting for the crossing time, it is not surprising that the finite F-P models are still slightly different from the Monte-Carlo models. It is also possible that the calibration of the escape parameter obtained by TPZ may not be applicable to large  $N$  clusters, since it was based on comparisons with smaller  $N$ -body simulations. It is reassuring to note, however, that the Monte-Carlo models, without introducing any new free parameters, have consistently lower mass loss rates compared to the infinite F-P models, and show better agreement with the finite F-P models.

### 3.3. Velocity and Pericenter Distribution of Escaping Stars

A major advantage of the Monte-Carlo method is that it allows the evolution of specific subsets of stars, or even individual stars, to be followed in detail. We use this capability to examine, for the first time in a cluster simulation with realistic  $N$ , the properties of stars that escape from the cluster through tidal stripping. We also examine the differences between the properties of escaping stars in clusters that reach core collapse, and those that disrupt. In Figure 9, we show the distribution of escaping stars for two different models ( $W_0 = 3$  and  $7$ , Family 1,  $\alpha = 2.5$ ). In each case, we show the distribution of the pericenter distance and the velocity at infinity for all the escaping stars. The velocity at infinity is computed as  $v_\infty = \sqrt{2(E - \phi_t)}$ , where  $E$  is the energy per unit mass of the star, and  $\phi_t$  is the potential at the tidal radius. We see that the distribution of pericenters is very broad, indicating that escape takes place from within the entire cluster, and not just near the tidal boundary. We see that the distribution of pericenters is more centrally peaked in the  $W_0 = 7$  model than in the  $W_0 = 3$  case. This is because the collapsing cluster has a hotter core, which can lead to a higher escape rate from the center. In a disrupting cluster, the core never gets very dense, and hence the distribution of pericenter distances drops sharply near the center. Note that the sizes of the cores are very different for the two clusters. The  $W_0 = 7$  cluster initially has a core radius of 0.2 (in virial units), which gets smaller as the cluster evolves, while the  $W_0 = 3$  cluster has an initial core radius of 0.5, which does not change significantly as the cluster evolves. The striking difference between the clusters, however, is in the velocity distribution of escaping stars. In the disrupting cluster, the distribution shows a wide range of energies for the escaping stars. But in the collapsing cluster, the distribution is bimodal, with two distinct peaks. The peak near zero velocity dominates the distribution. This peak represents stars escaping with close to the minimum energy, and hence from deep within the cluster. They must have very eccentric orbits in order to get beyond the tidal radius of the cluster. The smaller and wider peak represents the stars escaping from the outer region of the cluster. Since the density profile of a  $W_0 = 7$  King model is quite steep, the density in the region near the tidal radius is relatively low. This limits the overall tidal mass loss from the outer regions of the cluster.

The bimodal velocity distribution for the collapsing cluster shows that there are two funda-

mentally different mechanisms for escape. It also suggests that the single escape parameter used by TPZ to correct for the tidal mass loss rate in their finite F-P calculations may be insufficient in correcting for both types of escaping stars. This might account for the fact that TPZ find almost no change in the mass loss rate after introducing their  $\nu_{\text{esc}}$  parameter in core-collapsing models, while disrupting models show a significant difference.

### 3.4. Effect of Non-circular Orbits on Cluster Lifetimes

In all the calculations presented above (as in most previous numerical studies of globular cluster evolution), we assumed that the cluster remained in a circular orbit at a fixed distance from the center of the Galaxy. We also assumed that the cluster was born filling its Roche lobe in the tidal field of the Galaxy. Both of these assumptions are almost certainly unrealistic for the majority of clusters. However, one could argue that even for a cluster on an eccentric orbit, one might still be able to model the evolution using an appropriately *averaged* value of the tidal radius over the orbit of the cluster. We briefly explore the effect of an eccentric orbit, by comparing the evolution of one of our Monte-Carlo models ( $W_0 = 3$ ,  $\alpha = 2.5$ , Family 2) on a Roche-lobe filling circular orbit, and on an eccentric orbit. We assume that the *pericenter* distance of the eccentric orbit is equal to the radius of the circular orbit. This is to ensure that the cluster fills its Roche lobe at the same location in the models being compared.

In Figure 10, we show the evolution of the selected model for three different orbits. The leftmost line shows the evolution for the circular orbit. The rightmost line shows the evolution for an eccentric *Keplerian* orbit with a typical eccentricity of 0.6 (see, e.g., Odenkirchen et al. 1997). The Keplerian orbit assumes that the inferred mass of the Galaxy interior to the circular orbit is held fixed for the eccentric orbit as well. The intermediate line shows the evolution for an orbit in a more realistic potential for the Galaxy, which is still spherically symmetric, but with a constant circular velocity of  $220 \text{ km s}^{-1}$  in the region of the cluster orbit (Binney & Tremaine 1987). The orbit is chosen so that it has the same pericenter and apocenter distance as the Keplerian orbit. However, since the orbital velocity is higher, it has a shorter period compared to the Keplerian orbit. In each of the two eccentric orbits, we see that the cluster lifetime is extended slightly (by a factor of  $\sim 2$ ). Most of the mass loss takes place during the short time that the cluster spends near its pericenter, where it fills its Roche lobe. The Keplerian orbit gives the longest lifetime, since the cluster spends most of its time near its apocenter, where it does not fill its Roche lobe.

If we alternatively selected the orbit such that the cluster fills its Roche lobe at apocenter, instead of pericenter, the outcome would be obvious: the mass loss at pericenter would be considerably higher, leading to much more rapid disruption of the cluster compared to the circular orbit. This comparison indicates that the lifetime of a cluster can vary by a factor of a few, depending on the shape of its orbit. It also indicates that such corrections should be taken into account in building accurate numerical models of real clusters.

#### 4. Summary

We have calculated lifetimes of globular clusters in the Galactic environment using 2-D Monte-Carlo simulations with  $N = 10^5 - 3 \times 10^5$  King models, including the effects of a mass spectrum, mass loss in the Galactic tidal field, and stellar evolution. We have studied the evolution of King models with  $W_0 = 1, 3$ , and  $7$ , and with power-law mass functions  $m^{-\alpha}$ , with  $\alpha = 1.5, 2.5$ , and  $3.5$ , up to core collapse, or disruption, whichever occurs first. In our broad survey of cluster lifetimes, we find very good overall agreement between our Monte-Carlo models and the 2-D F-P models of TPZ for all 36 models studied. This is very reassuring, since it is impossible to verify such results using direct  $N$ -body integrations for a realistic number of stars. The Monte-Carlo method has been shown to be a robust alternative for studying the evolution of multi-component clusters. It is particularly well suited to studying finite, but large- $N$  systems, including many different processes, such as tidal stripping and stellar evolution, which operate on different timescales. We find that our Monte-Carlo models are in better agreement with the finite- $N$  F-P models of TPZ, compared to their standard F-P ( $N \rightarrow \infty$ ) models, although our models still appear to have a slightly lower overall mass loss rate.

Even though our simulations are getting more sophisticated and realistic with the inclusion of most of the dominant effects, there still remain substantial difficulties in relating our results directly to observed clusters. We ignore several important effects in these calculations, including the tidal shock heating of the cluster due to passages through the Galactic disk, and the presence of primordial binaries, which can support the core against collapse. In recent studies using 1-D F-P calculations, it has been shown that shock heating and shock-induced relaxation of clusters caused by repeated close passages near the bulge, and through the disk of the Galaxy can be as important as 2-body relaxation for their overall dynamical evolution (Gnedin, Lee, & Ostriker 1999). In addition, the initial mass function of clusters is poorly constrained observationally. In our study, we assume that clusters begin their lives filling their Roche lobes. But, as we have shown, a cluster on an eccentric orbit may spend most of its time further away in the galaxy, where it might not fill its Roche lobe. This can lead to somewhat longer lifetimes.

The broad survey of cluster lifetimes presented here, and the similar effort by TPZ, lay the foundations for more detailed calculations, which may one day allow us to conduct reliable population synthesis studies to understand in detail the history, and predict the future evolution, of the Galactic globular cluster system.

We are very grateful to Simon Portegies Zwart for insightful comments and helpful discussions. We are also grateful to Koji Takahashi for kindly providing valuable data and answering numerous questions. This work was supported by NSF Grant AST-9618116 and NASA ATP Grant NAG5-8460. F.A.R. was supported in part by an Alfred P. Sloan Research Fellowship. This work was also supported by the National Computational Science Alliance and utilized the SGI/Cray Origin2000 supercomputer at Boston University.

## REFERENCES

Binney, J., & Tremaine, S. 1987, Galactic Dynamics (Princeton, PUP)

Chernoff, D. F. & Weinberg, M. D. 1990, ApJ, 351, 121

Cohn, H. 1979, ApJ, 234, 1036

Cohn, H. 1980, ApJ, 242, 765

Druckier, G. A. 1995, ApJS, 100, 347

Druckier, G. A., Cohn, H. N., Lugger, P. M., & Yong, H. 1999, ApJ, 518, 233

Fukushige, T., & Heggie, D. C. 1995, MNRAS, 276, 206

Gao, B., Goodman, J., Cohn, H., & Murphy, B. 1991, ApJ, 370, 567

Gnedin, O. Y., Lee, H. M., & Ostriker, J. P. 1999, ApJ, 522, 935

Goodman, J., & Hut, P. 1989, Nature, 339, 40

Heggie, D. C., Giersz, M., Spurzem, R., & Takahashi, K. 1999, in Highlights of Astronomy, vol. 11, ed. J. Andersen, 591

Henon, M. 1971a, Ap. Space Sci., 13, 284

Henon, M. 1971b, Ap. Space Sci., 14, 151

Hut, P., McMillan, S., & Romani, R. W. 1992, ApJ, 389, 527

Iben, I., & Renzini, A. 1983, Ann. Rev. Astr. Ap., 21, 271

Joshi, K. J., Rasio, F. A., & Portegies Zwart, S. 1999 (Paper I), ApJ, submitted [astro-ph/9909115]

Lee, H. M., & Ostriker, J. P. 1987, ApJ, 322, 123

Makino, J., Taiji, M., Ebisuzaki, T., & Sugimoto, D. 1997, ApJ, 480, 432

McMillan S. L. W., & Hut P. 1994, ApJ, 427, 793

McMillan S. L. W., Hut P., & Makino, J. 1990, ApJ, 362, 522

Meylan, G., & Heggie, D. C. 1997, A&A Rev. 8, 1

Miller, G. E., & Scalo, J. M. 1979, ApJ, 41, 513

Odenkirchen, M., Brosche, P., Geffert, M., & Tucholke, H. J. 1997, New Astronomy, 2, 477

Portegies Zwart, S., Hut, P., Makino, J., & McMillan, S.L.W. 1998, A&A, 337, 363

Quinlan, G.D. 1996, *New Astronomy*, 1, 255

Ross, D. J., & Mennim, A., & Heggie, D. C. 1997, *MNRAS*, 284, 811

Spitzer, L. 1987, *Dynamical Evolution of Globular Clusters* (Princeton: Princeton University Press)

Spitzer, L., & Mathieu, R. D. 1980, *ApJ*, 241, 618

Takahashi, K. 1995, *PASJ*, 47, 561

Takahashi, K. 1996, *PASJ*, 48, 691

Takahashi, K. 1997, *PASJ*, 49, 547

Takahashi, K., & Portegies Zwart, S. F. 1998, *ApJ*, 503, L49

Takahashi, K., & Portegies Zwart, S. F. 1999 (TPZ), *ApJ*, submitted [astro-ph/9903366]

Table 1. Main-Sequence Lifetimes and Remnant Masses <sup>a</sup>

$m_{initial}[\text{M}_\odot]$	$\log(\tau_{\text{MS}}[\text{yr}])$	$m_{final}[\text{M}_\odot]$
0.40	11.3	0.40
0.60	10.7	0.49
0.80	10.2	0.54
1.00	9.89	0.58
2.00	8.80	0.80
4.00	7.95	1.24
8.00	7.34	0.00
15.00	6.93	1.40

<sup>a</sup>For consistency, we use the same main-sequence lifetimes and remnant masses as CW, from Iben & Renzini (1983) and Miller & Scalo (1979).

Table 2. Family Properties <sup>a</sup>

Family	$F$	$t_{\text{rh}}$ [Gyr]	$R_g$ [kpc]
1	$5.00 \times 10^4$	2.4	5.8
2	$1.32 \times 10^5$	6.4	15
3	$2.25 \times 10^5$	11	26
4	$5.93 \times 10^5$	29	68

<sup>a</sup>Sample parameters for Families 1–4, for a  $W_0 = 3$  King model, with  $\bar{m} = 1\text{M}_\odot$ , and  $N = 10^5$ . Distance to the Galactic center  $R_g$  is computed assuming that the cluster is in a circular orbit, filling its Roche lobe at all times.

Table 3. Comparison of Monte-Carlo results with 1-D Fokker-Planck calculations <sup>a</sup>

$W_0$	$\alpha$	Family							
		1		2		3		4	
		CW	MC	CW	MC	CW	MC	CW	MC
1 .....	1.5	D	D	D	D	D	D	D	D
		0.0092	0.03	0.0094	0.03	0.0093	0.03	0.0092	0.03
		0	0	0	0	0	0	0	0
	2.5	D	D	D	D	D	D	D	D
		0.034	0.55	0.034	0.62	0.035	0.66	0.034	0.70
		0	0	0	0	0	0	0	0
	3.5	D	C	D	C	D	D	D	D
		2.5	27	2.9	52	3.1	58	3.2	85
		0	0.12	0	0.02	0	0	0	0
3 .....	1.5	D	D	D	D	D	D	D	D
		0.014	0.032	0.014	0.032	0.014	0.032	0.014	0.032
		0	0	0	0	0	0	0	0
	2.5	D	D	D	D	D	D	D	D
		0.28	5.2	0.29	8.8	0.29	10	0.29	11
		0	0	0	0	0	0	0	0
	3.5	C	C	C	C	D	C	D	C
		21.5	31	44.4	90	42.3	130	43.5	390
		0.078	0.28	0.035	0.23	0	0.20	0	0.18
7 .....	1.5	D	C	D	C	D	C	D	C
		1.0	3.1	3.0	7.7	4.2	12	5.9	27
		0	0.08	0	0.05	0	0.05	0	0.05
	2.5	C	C	C	C	C	C	C	C
		9.6	3	22.5	6	35.5	10	83.1	20
		0.26	0.60	0.26	0.55	0.26	0.57	0.25	0.50
	3.5	C	C	C	C	C	C	C	C
		10.5	6.0	31.1	20	51.3	38	131.3	90
		0.57	0.80	0.51	0.70	0.48	0.68	0.49	0.67

<sup>a</sup> The results of Chernoff & Weinberg (1990, CW) are taken from their Table 5. MC denotes our Monte-Carlo results. The first line describes the final state of the cluster at the end of the simulation: C indicates core collapse, while D indicates disruption. The second line gives the time to core collapse or disruption, in units of  $10^9$  yr. The third line gives the final cluster mass in units of the initial mass.

Table 4. Comparison of disruption times for infinite ( $N \rightarrow \infty$ ) and finite ( $N = 3 \times 10^5$ ) F-P models from TPZ with Monte-Carlo ( $N = 3 \times 10^5$ ) models.<sup>a</sup>

	Fokker-Planck ( $N \rightarrow \infty$ )	Fokker-Planck ( $N = 3 \times 10^5$ )	Monte-Carlo ( $N = 3 \times 10^5$ )
$W_0 = 1$ , Family 1	$3.1 \times 10^8$ yr	$4.8 \times 10^8$ yr	$5.5 \times 10^8$ yr
$W_0 = 1$ , Family 4	$3.3 \times 10^8$ yr	$12.2 \times 10^8$ yr	$7.0 \times 10^8$ yr
$W_0 = 3$ , Family 1	$2.2 \times 10^9$ yr	$2.6 \times 10^9$ yr	$5.3 \times 10^9$ yr
$W_0 = 3$ , Family 4	$3.1 \times 10^9$ yr	$5.3 \times 10^9$ yr	$10.1 \times 10^9$ yr

<sup>a</sup>All models have a mass function  $m^{-\alpha}$  with  $\alpha = 2.5$  ( $\bar{m} = 1\text{M}_\odot$ ).

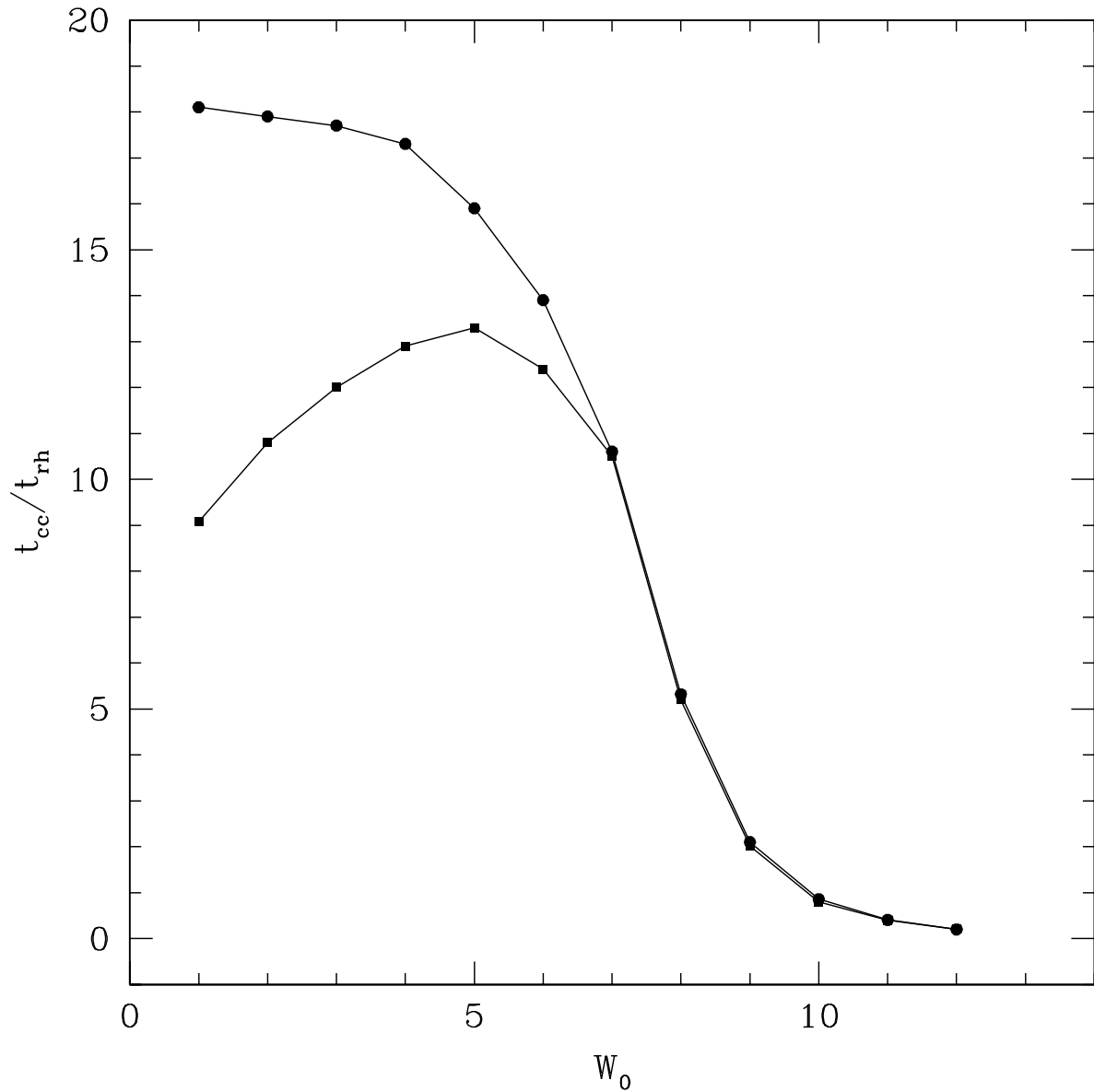


Fig. 1.— Comparison of core-collapse times for  $W_0 = 1 - 12$  single-component King models. Isolated models, i.e., without an enforced tidal boundary, are indicated by solid circles, while tidally truncated models are indicated by squares.

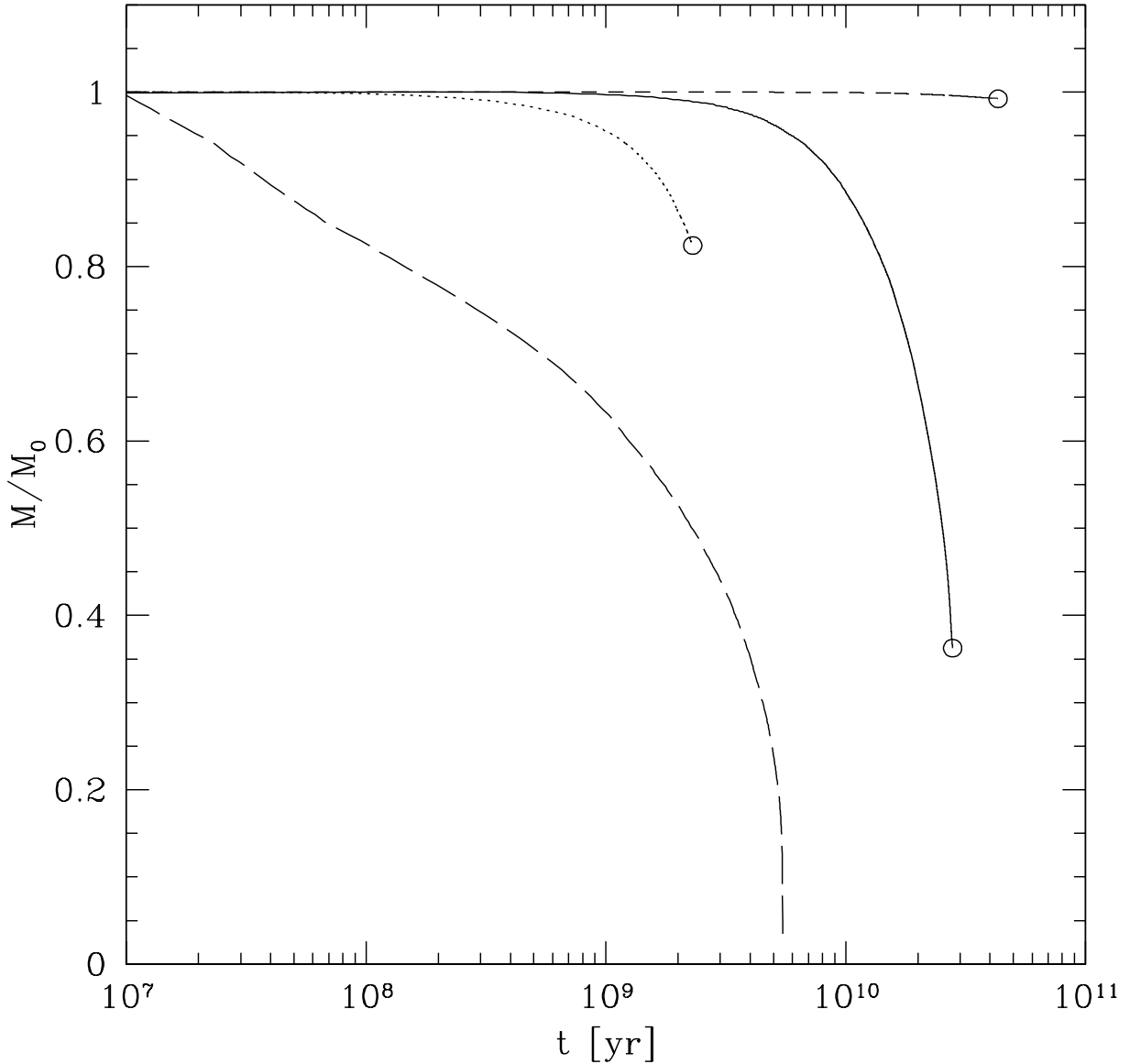


Fig. 2.— Comparison of the mass loss rate in a  $W_0 = 3$  King model due to a tidal boundary, a power-law mass spectrum, and stellar evolution. The mass of the cluster, in units of the initial mass  $M_0$ , is shown as a function of time. The solid and short-dashed lines are for a single-component model, with and without a tidal boundary, respectively. The dotted line shows a model with a power-law mass spectrum, with  $\alpha = 2.5$ , and a tidal boundary. The long-dashed line is for a more realistic model with a tidal boundary, power-law mass spectrum, and stellar evolution. The circle at the end of the line indicates core collapse. The line without a circle indicates disruption of the cluster.

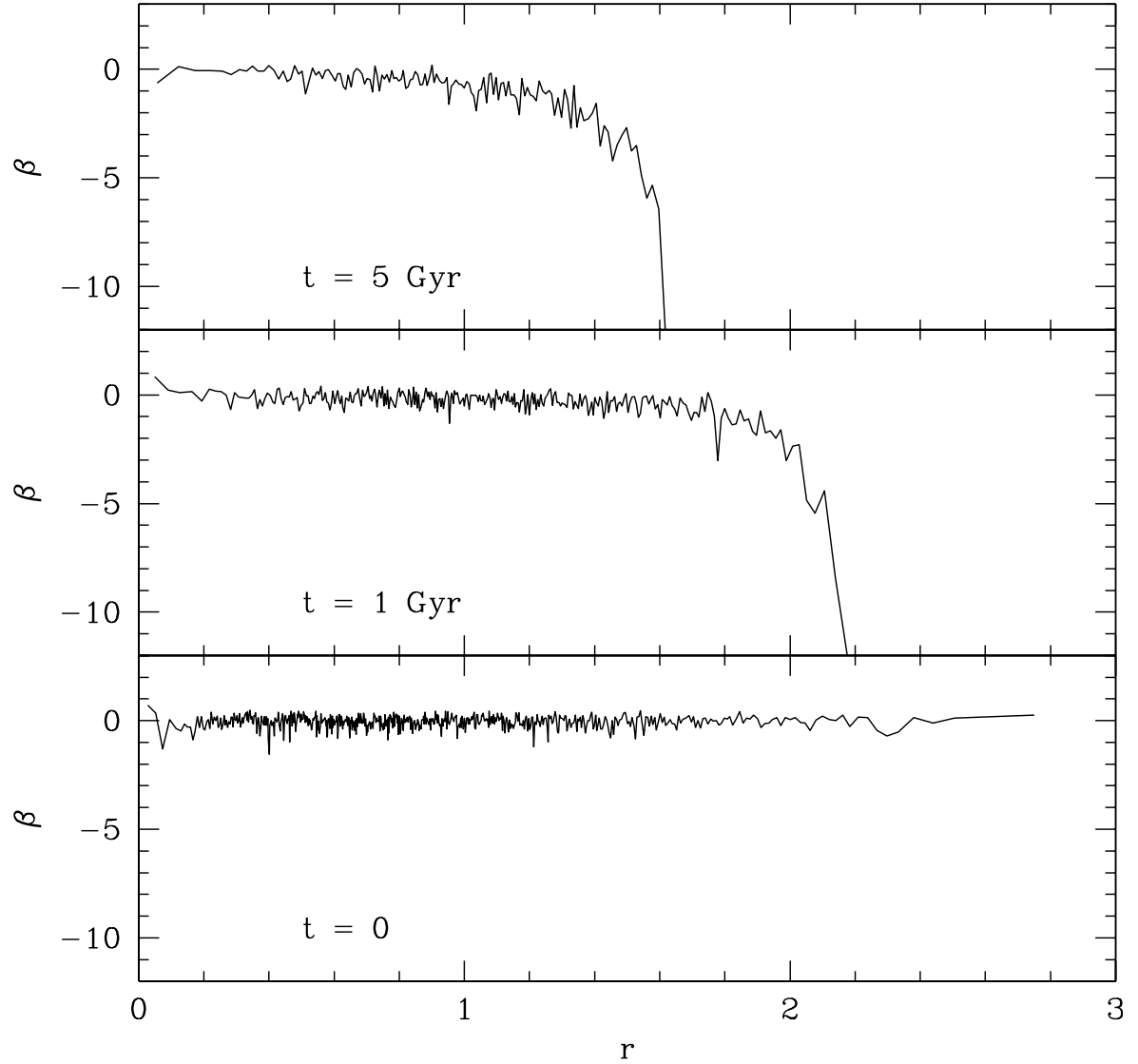


Fig. 3.— Evolution of the anisotropy parameter  $\beta = 1 - \sigma_t^2 / \sigma_r^2$  for a  $W_0 = 3$  King model ( $\alpha = 2.5$ , Family 1). The bottom frame shows the initial isotropic King model. The top frame shows the anisotropy just before disruption. The radius is in units of the virial radius. Stars on highly eccentric orbits with large apocenter distances in the cluster are preferentially removed, causing  $\sigma_t^2 / \sigma_r^2$  to increase in the outer region.

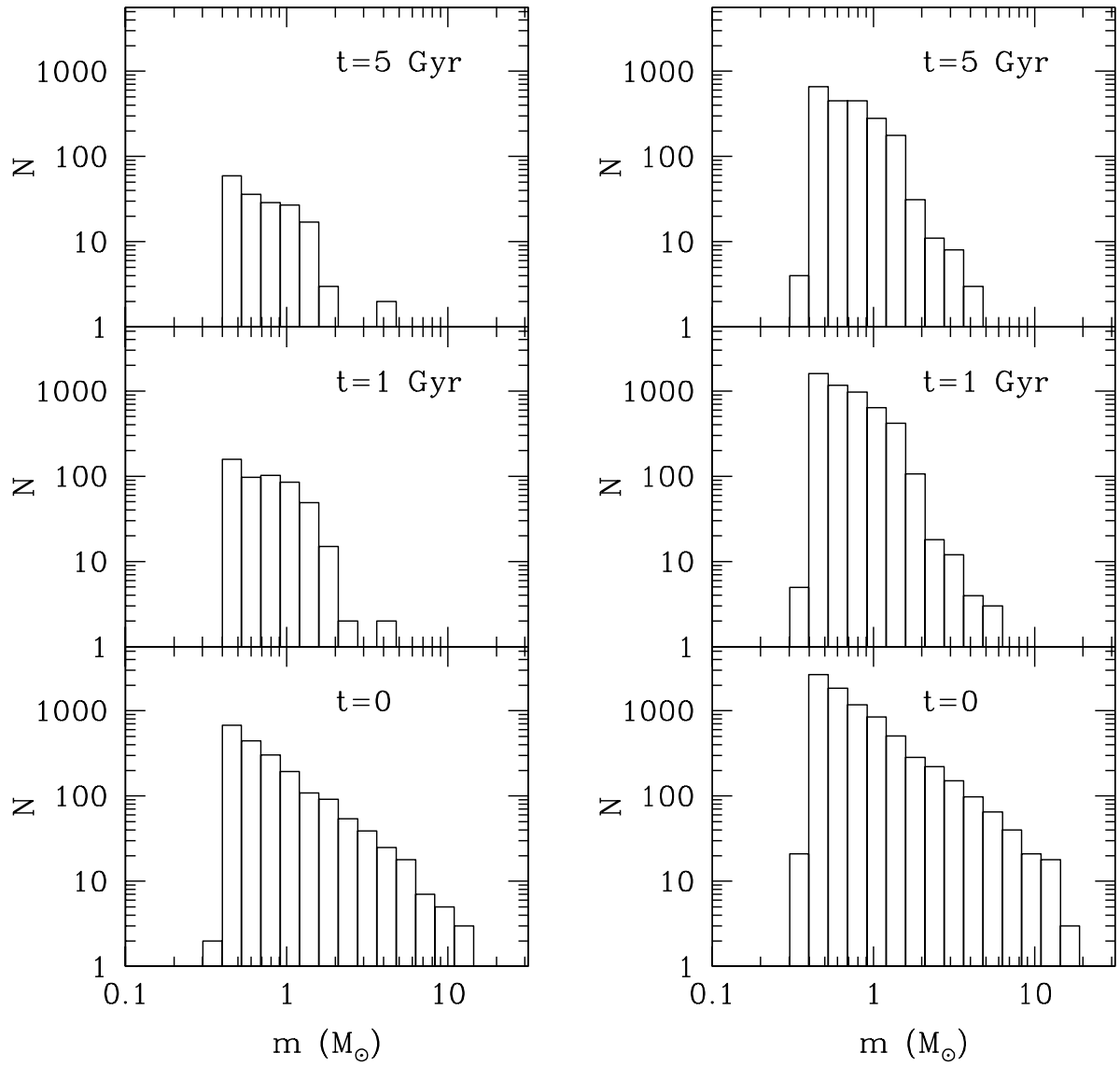


Fig. 4.— Evolution of the mass spectrum for a  $W_0 = 3$  King model with an initial power-law mass function  $m^{-\alpha}$ , with  $\alpha = 2.5$ , Family 1. The mass spectra in the core (left panels), and at the half-mass radius (right panels) are shown at 1 Gyr, and 5 Gyr. The mass spectrum flattens as a result of stellar evolution, mass segregation and evaporation.

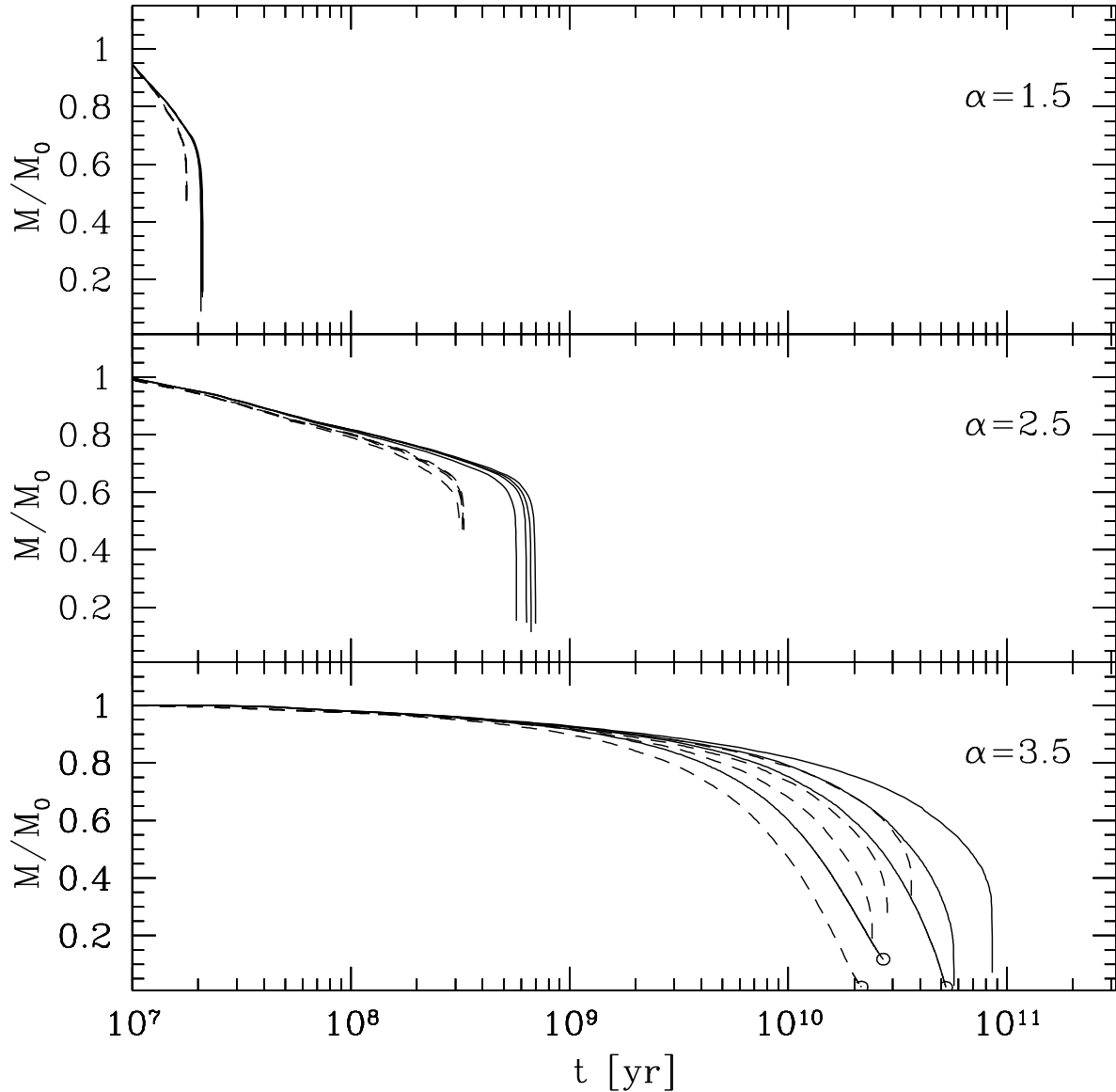


Fig. 5.— Evolution of the total mass with time for  $W_0 = 1$  King models, Families 1–4. Comparison is made between our Monte-Carlo models (solid lines) and 2-D F-P models (dashed lines). The three panels show results for different values of the exponent  $\alpha$  of the *initial* power-law mass function ( $m^{-\alpha}$ ). The four lines for each case, represent Families 1 – 4, from left to right. We indicate a core collapsed model with a circle at the end of the line. Lines without a circle at the end indicate disruption.

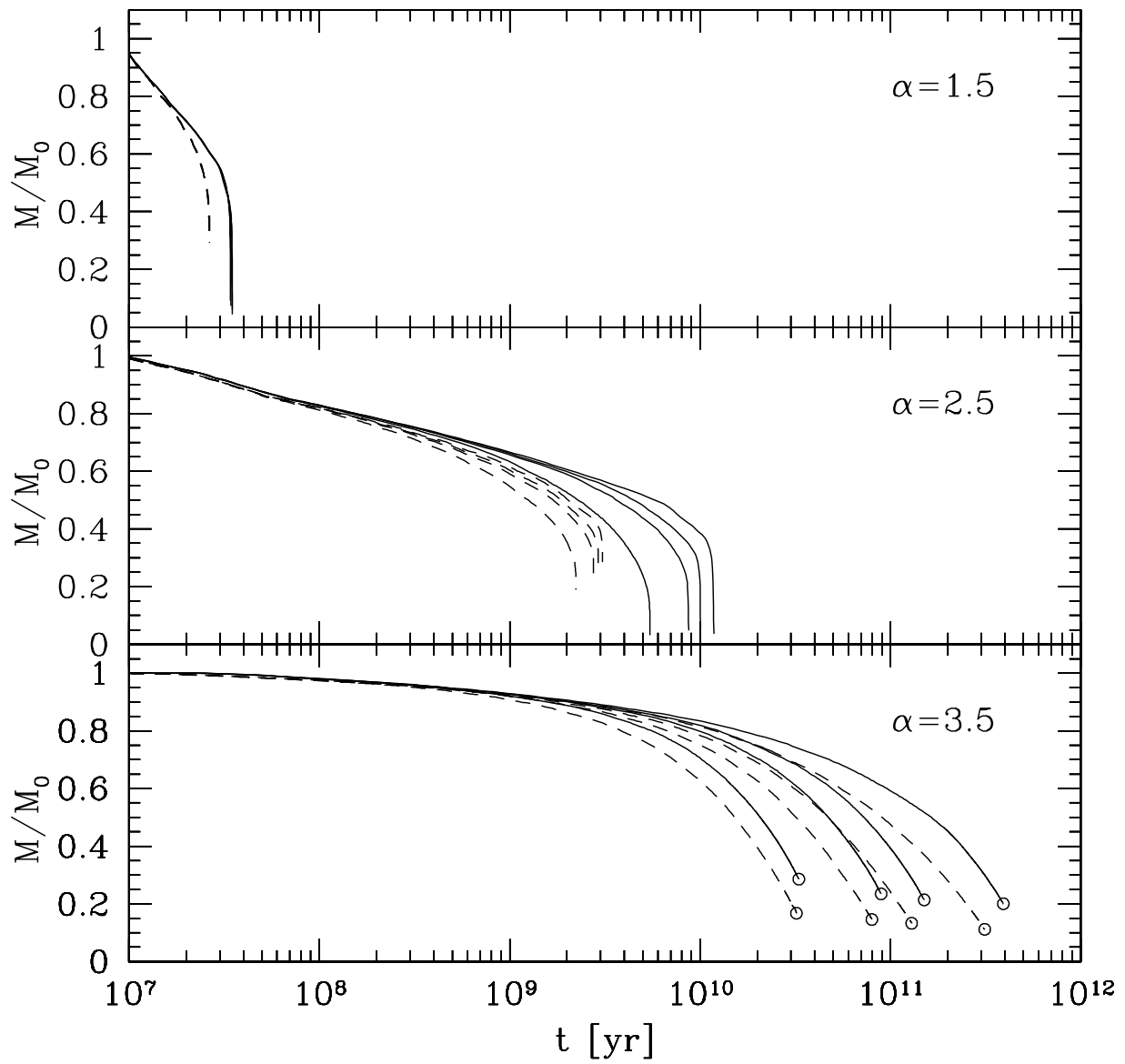


Fig. 6.— Same as Figure 5, but for  $W_0 = 3$  King models.

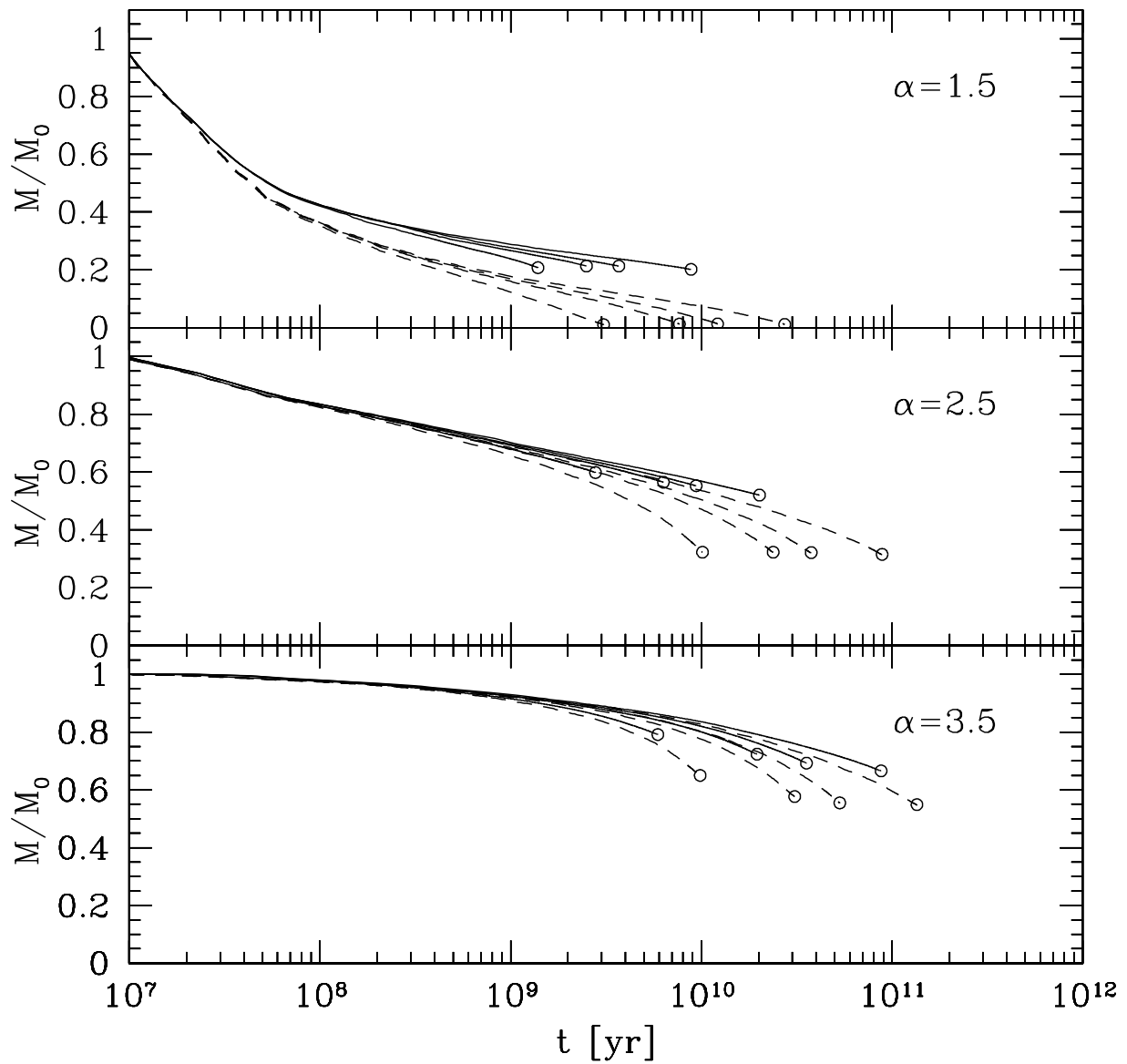


Fig. 7.— Same as Figure 5, but for  $W_0 = 7$  King models.

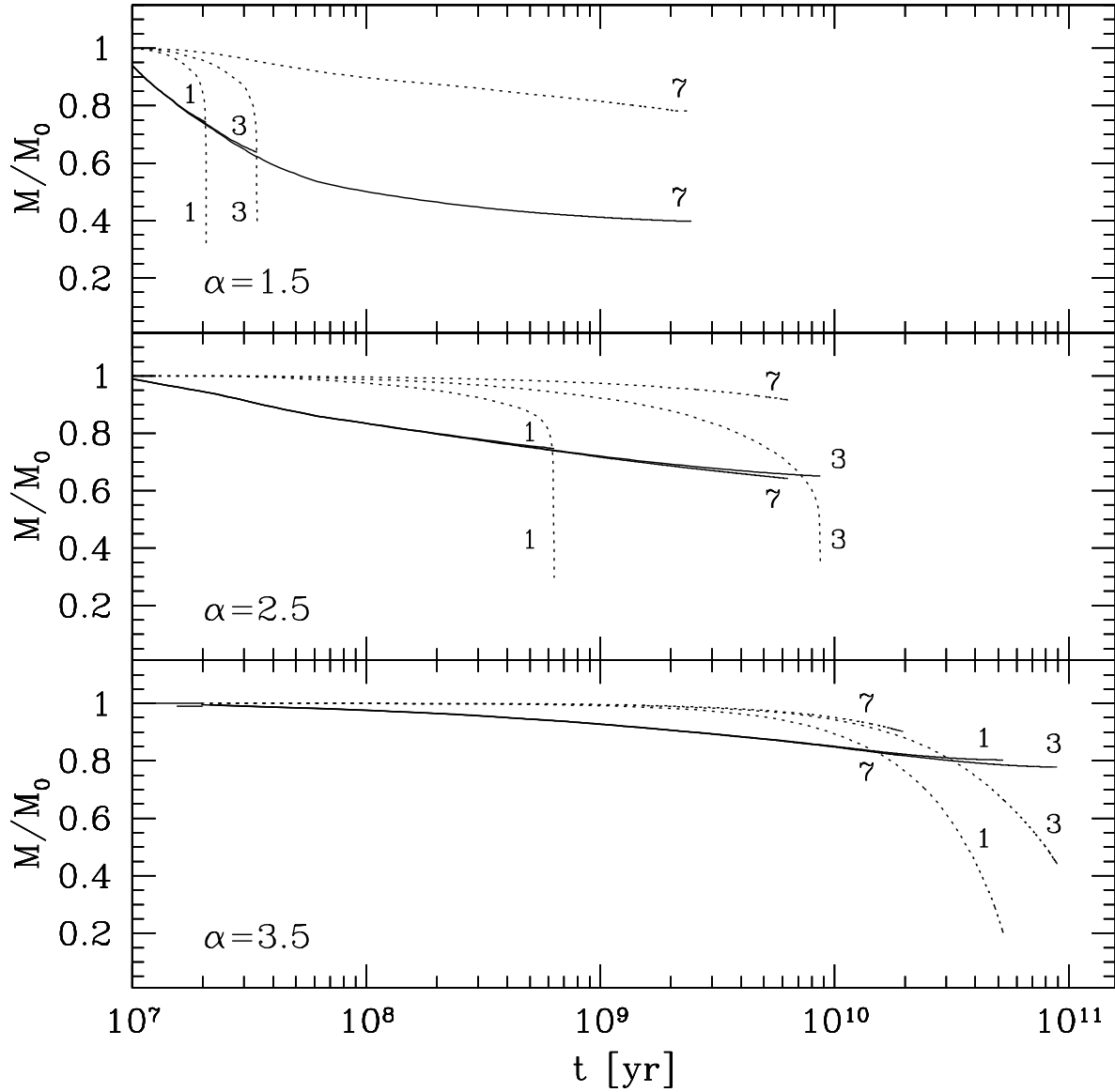


Fig. 8.— Comparison of the mass loss due to stellar evolution (solid lines), and mass loss due to tidal stripping of stars (dotted lines), for  $W_0 = 1, 3$ , and  $7$  King models, with initial mass functions  $m^{-\alpha}$ ,  $\alpha = 1.5, 2.5$ , and  $3.5$ . The numbers  $1, 3$ , and  $7$  next to the lines indicate an initial model with  $W_0 = 1, 3$ , and  $7$ , respectively. All models belong to Family 2. Results for other Families show similar trends. Note that the mass loss due to stellar evolution is almost independent of  $W_0$  (as expected), but the tidal mass loss varies significantly with  $W_0$ . In the early phases of evolution, the mass loss due to stellar evolution dominates, while in the later stages, tidal stripping of stars is the dominant mechanism.

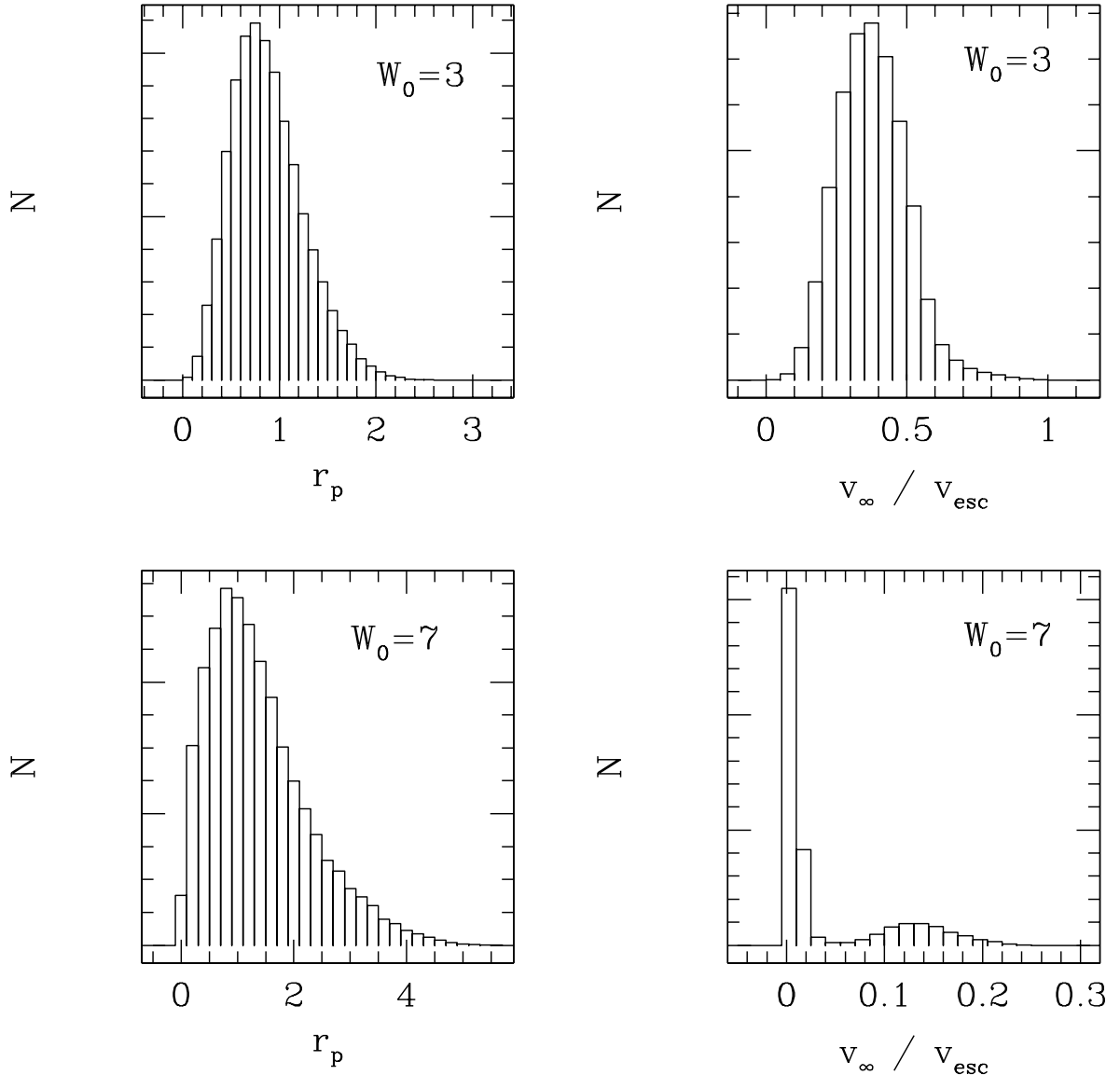


Fig. 9.— Distribution of the pericenter distance and velocity of the escaping stars, for two different King models:  $W_0 = 3$  and  $7$  (Family 1,  $\alpha = 2.5$ ). The  $W_0 = 3$  model disrupts, while the  $W_0 = 7$  model undergoes core collapse. The pericenter distance is given in units of the virial radius of the cluster. The velocity “at infinity” is computed as  $v_\infty = \sqrt{2(E - \phi_t)}$ , where  $E$  is the energy per unit mass of the star, and  $\phi_t$  is the potential at the tidal radius. The escape velocity is defined as  $v_{\text{esc}} = \sqrt{2(\phi_t - \phi_0)}$ , where  $\phi_0$  is the potential at the center of the cluster. While the distribution of pericenter distances of escaping stars looks quite similar in the two clusters, the distribution of velocities is strikingly different. In the disrupting cluster ( $W_0 = 3$ ), the escaping stars have a wide range of energies, whereas in the collapsing cluster ( $W_0 = 7$ ), most stars escape with close to the minimum energy. The velocity distribution in the collapsing cluster also shows *two* distinct peaks, indicating that there are two fundamentally different mechanisms for escape.

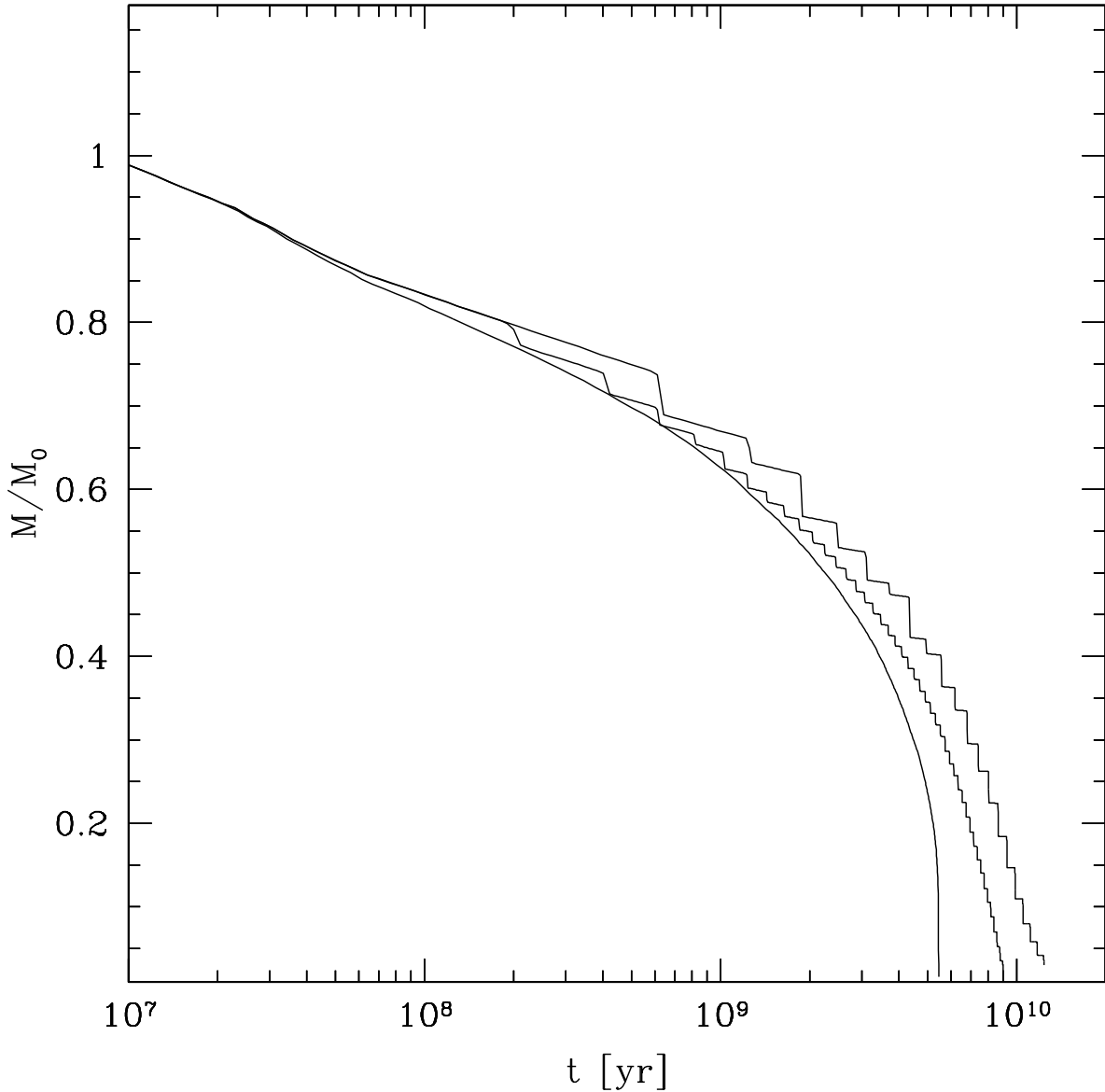


Fig. 10.— Comparison of the mass loss for a  $W_0 = 3$ ,  $\alpha = 2.5$  (Family 2) King model, on three different assumed orbits in the Galaxy. The leftmost line shows a circular orbit, with radius  $R_g = 5.76$  kpc. The cluster is assumed to fill its Roche lobe at this distance. The rightmost line shows a Keplerian elliptical orbit with eccentricity 0.6 and a *pericenter* distance of 5.76 kpc. Since the cluster on such an orbit spends most of its time at a larger distance, the cluster does not fill its Roche lobe at all times. This results in a sharp mass loss every time the cluster approaches pericenter. The lifetime of the cluster is longer by almost a factor of 2. The intermediate line is for an orbit in a more realistic Galactic potential, with a constant circular velocity of  $220 \text{ km s}^{-1}$ , with the same pericenter and apocenter distances as for the Keplerian elliptical orbit. The orbit is no longer elliptical, and the orbital period is shorter, resulting in a lifetime that is intermediate between the circular and elliptical cases.